This is a peer-reviewed, accepted author manuscript of the following article: Chaganti, P., Yuan, W., Xu, L., Zhang, M., Hodge, E., Fitzgerald, J., & McKeever, P. (2024). Transient analysis of HVDC HTS cable in power grid using discretized electrical-thermal model. IEEE Transactions on Applied Superconductivity, 34(3), Article 4803806. https://doi.org/10.1109/tasc.2024.3370896

Transient Analysis of HVDC HTS Cable in Power Grid Using Discretized Electrical-Thermal Model

Pavan Chaganti, Weijia Yuan, *Senior Member, IEEE,* Lie Xu, *Senior Member, IEEE,* Min Zhang, *Member, IEEE,* Eoin Hodge, John Fitzgerald and Paul McKeever

***Abstract*— High-temperature superconductor (HTS) power cables hold immense potential for efficient, low-loss, high-current-density, and compact power transmission. However, the susceptibility of HTS cables to faults in the grid, resulting in quenching or permanent damage due to joule heating, poses a critical challenge for their real-world resilience. To address this, we developed a discretized electrical-thermal model using MATLAB/SIMSCAPE, partitioning the cable into discrete blocks to understand transient conditions and implement preventive measures in long-distance superconducting cable power transmission. The model should have the flexibility to change the fault location along the length of the cable, including the HTS and copper former and LN_2 layers. In our simulations, we examined a 100 km long 100 kV/10 kA HVDC HTS cable, varying the fault locations to 1, 5, 50, and 100 km. This investigation unveiled significant variations in both thermal and electrical behaviour, more impact was observed when faults occurred in proximity to the voltage source. This study underscores the benefits of integrating Superconducting Fault Current Limiters (SFCL) with HTS cables in the network, showcasing load sharing between the superconductor and copper former during steady and transient state operation, HTS quench and recovery time.**

***Index Terms*— Superconducting power cable, HTS, Line to ground (LG) Fault, and Superconducting fault current limiter (SFCL).**

I. INTRODUCTION

THE demand for clean and reliable energy has led to significant advancements in power transmission systems. The utilization of offshore wind for clean energy generation has experienced significant growth. Currently, offshore wind farms are being constructed at great distances from the shore. An example of this is the Hornsea wind farm project, which is located 120 km from the Yorkshire coast and has a capacity of 1.2 GW. This project began full operation in 2019 and is capable of powering over one million homes.

The traditional method of using XLPE copper cables to handle higher power capacities involves raising the voltage levels to Ultra High Voltage (UHV)—to minimize energy losses and fulfill the increasing power demands. This approach results in the need for greater insulation quantities within the cables and also an increase in converters, switchgear and circuit breaker size.

One promising solution to that was the use of the superconductor power cable for the offshore power grids. The utilization of superconducting technology allows a significant increase in current capacity, up to 5 to 6 times more, due to its resistance-free nature. consequently, the voltage level drops, resulting in a reduction in the amount of insulation required for the cable.

Several demo projects are using superconductors, extending this new technology in modern power grids due to its superior characteristics. In 2007, a 600-meter-long HTS cable with a rating of 138 kV and 2400 amps was commissioned in Long Island, USA [1]. In Hannover, Germany the ENDESA super cable was developed for a length of 30 meters with a 3200 A rated current. It is implemented with the scope of application in a medium voltage grid of 25 kV with a transmission capacity of 138 MVA [2]. In Essen Germany, an AC HTS cable of 1 km length was installed with a capacity of 10 kV/ 2.4 kA [3]. In Albany, in the power grid, a 350 m HTS cable was installed with operating conditions of 34.5 kV and 800 A [4]. In Ishikari, Japan a 500 m and 1000 m DC HTS was installed [5]. In Gongyi, Henan a 360-meter-long DC HTS cable was installed at Zhongfu Industrial Co., Ltd, with a capacity of 10 kA and 1300 V [6]. In St.Petersburg, Russia a DC HTS cable link was developed with a capacity of 2.5 kA, 20 kV, and 50 MW for a length of 2.5 km [7]. Since 2015 in the KEPCO grid, South Korean HVDC cable of 500MW/80 kV was in operation [8], [9]. In 2017, a prototype of a 30 m long medium voltage 3-phase AC concentric HTS cable, rated at 10 kV/2.5 kArms with a current capacity (Ic) of 6 kA per phase, was developed for grid installation. Following a successful trial, Shenzhen Power Supply installed a 400-meter-long HTS cable at the Ping'an Financial Center on September 28, 2021, which has been operating smoothly [10], [11]. A demo project of 1.2 km, 35 kV/2.2 kA Shanghai superconductor power cable began in 2019 and completed both the prototype and commissioning test by November 2021 [12]. Another significant endeavour, supported by the New Energy Technology Development Organization (NEDO) and BASF Japan Ltd., showcased a 6 kV/3 kA triaxial HTS cable. This cable was specifically deployed in the chemical plant grid of BASF to bypass the need for substations [13]. In August 2021, in Chicago, integrated the AMSC's AC power cable of 200 meters into an electric grid with a capacity of 62 MW/12 kV/3 kA [14].

This work was supported by the collaboration project between SuperNode and the Offshore Renewable Energy Catapult as part of the Research Programme of the OREC Electrical Infrastructure Research Hub.
(Corresponding authors: Pavan Chaganti; Weijia Yuan.)
Pavan Chaganti, Min Zhang, Lie Xu, Weijia Yuan are with the University of Strathclyde, Glasgow, G1 1RD, U.K.
(e-mail: lakshmana.chaganti@strath.ac.uk; weijia.yuan@strath.ac.uk)
Eoin Hodge and John Fitzgerald are with the SuperNode, Belfield, Dublin 4 D04 V2P1, Ireland
Paul McKeever is with the Offshore Renewable Energy Catapult (OREC), NE24 1LZ Blyth, Northumberland, U.K

Superconductors offer several advantages over traditional cables. However, a comprehensive analysis is essential to assess its performance in the event of a fault. During a fault, joule heating intensifies, causing a temperature increase that can result in either quenching without damaging the superconductor or permanent damage. Using modelling methods is crucial for predicting and studying HTS power systems' behaviour, offering a cost-effective and time-saving alternative to physical experiments. In safeguarding the HTS cable and the power electronic converters from potential damage during faults, an SFCL proves beneficial in mitigating high inrush currents in the HTS cable. Different types of SFCLs are under investigation and are in operation within power grids [15]–[20].

To study how HTS cables behave, researchers use numerical models created with tools like MATLAB, PSCAD, ANSYS, and COMSOL [21]–[25]. The models built in MATLAB, and PSCAD are simplified models, while those in ANSYS and COMSOL are extremely complex and time-consuming to run. Inbuilt components, in these tools, typically offer resistive components that exhibit linear behaviour with temperature, but the HTS cables have nonlinear resistance affected by factors like cable current, critical current, and temperature. To address this, we build SIMSCAPE components in MATLAB/SIMSCAPE one for HTS cable and the other for SFCL. These components incorporate thermal, hydraulic, and electrical equations specific to HTS cable, and SFCL. This paper aims to investigate how the location of the fault impacts the quench behaviour of the superconductor cable and the distribution of current within the HVDC superconductor power cable.

II. Methodology

The superconductor tape and cable structure are shown in Fig. 1(a) and 1(b). The flow chart in Fig. 1(c) gives in detail the procedure for the design of the cable electro-thermal model in MATLAB/SIMSCAPE. The tape twist angle and its twist pitch length (P) are shown in Fig. 1(d). The cable specifications are mentioned in Table 1. The resistance of the HTS was calculated by the EJ-power law using the Ic vs temperature data from the reference [26]. The model considered the conduction, convection, and heat transfer between the layers in radial and axial directions.

The inductance of the superconductor cable depends on the twist pitch of the superconductor tapes, and the radius and diameter of the cable. The self-inductance of the HTS cable-based pitch angle (β_i) is as follows [27], [28].

$$L_{self\_hts} = \frac{\mu_0}{4\pi} tan^2(\beta_i) + \frac{\mu_0}{2\pi} ln\,(\frac{r_4}{r_2}) \quad (1)$$

The mutual inductance between the HTS layer and copper former was calculated by applying Amperes law and total enclosed magnetic energy.

$$M = \frac{\mu_0}{\pi} \log\left(\frac{r_4}{r_3}\right) + \frac{\mu_0}{\pi}(r_2 - r_1) \quad (2)$$

The voltage of the superconductor layer and copper former are as follows:

$$V_{hts} = i_{hts}R_{hts} + L_{self\_hts}\frac{di_{hts}}{dt} + M\frac{di_{cu}}{dt} \quad (3)$$

$$V_{cu} = i_{cu}R_{cu} + L_{self\_cu}\frac{di_{cu}}{dt} + M\frac{di_{hts}}{dt} \quad (4)$$

Where r_1 to r_9 are the radius of the superconductor cable layers as shown in Fig. 1(b). where μ_0 (vacuum permeability coefficient) $= 4\pi 10^{-7}\text{N/A}^2$ and V_{hts}, i_{hts}, and R_{hts} are the voltage, current, and resistance of the HTS layer. Similarly, for the copper former with subscript cu.

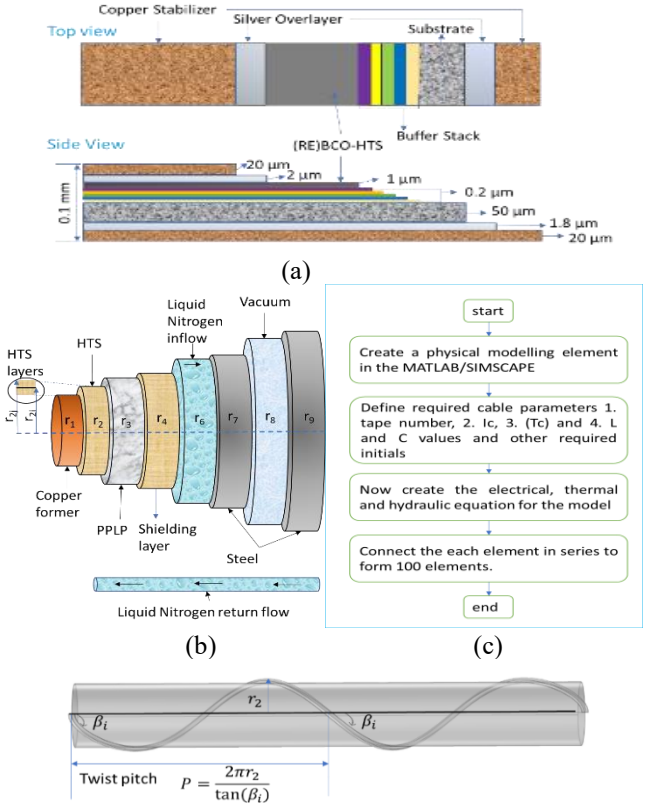

Fig. 1. (a) top and side view of HTS tape, (b) HTS cable structure, (c) Flow chart of the cable component design in the MATLAB/SIMSCAPE, and (d) HTS tape twist pitch schematic view

TABLE 1
HTS cable parameters when the pitch angle is 20

Parameter	Value
Critical current (Ic)	22 kA@70K
Capacitance (C)	0.191 µF/km
Self-inductance of HTS (L_{self_hts})	0.0579 mH/km
Self-inductance of former (L_{self_cu})	0.188 mH/km
Mutual inductance (M)	0.0455 mH/km
Number of tapes	74
Cable length	100 km

The cable components are discretized both radially and axially, illustrated in Fig. 2. Utilizing the first law of thermodynamics, as outlined in reference [29], we applied it to these discretized elements.

Heat conduction takes place within the solid layers along

both radial and axial directions. Equation 5 represents the heat transfer through conduction within the same material layer in the axial direction, while equation 6 expresses the conduction between different materials in the radial direction accoridngly.

$$Q_{cond,i,i+1} = \frac{k_r A_r (T_r^{i+1} - 2T_r^i + T_r^{i-1})}{\Delta l} \quad (5)$$

$$Q_{cond,r2,r3} = (T_{r3}^i - T_{r2}^i)\left(\frac{\ln\left(\frac{2r_2}{r_1+r_2}\right)}{2\pi k_{r2}\Delta l} + \frac{\ln\left(\frac{r_2+r_3}{2r_2}\right)}{2\pi k_{r3}\Delta l}\right)^{-1} \quad (6)$$

The convection heat transfer happens either in the liquid medium or between the liquid and solid materials. The convection heat transfer in the radial direction is given in equation 7 and the axial direction is given in equation 8.

$$Q_{conv,r4,r5} = -hA_{r4,r5}\left(T_{r5}^i - T_{r4}^i\right) \quad (7)$$

$$Q_{conv,i,i+1} = mc_p(T_r^{i+1} - T_r^i) \quad (8)$$

The heat through the radiation between the layers is given in equation 9.

$$Q_{radiation} = -\frac{\varepsilon_1}{1-\varepsilon_1}A_{r6}\left(B_1 - \sigma(T_{r6}^i)^4\right) + \frac{\varepsilon_2}{1-\varepsilon_2}A_{r7}\left(\sigma(T_{r7}^i)^4 - B_2\right) \quad (9)$$

Where h is the heat transfer coefficient A_r is the cross-section area, k_r is thermal conductivity, Δl is the element size, m is mass flow in kg/s, and c_p is the specific heat (J/kg-K). Where $\varepsilon_1$and ε_2 are the material emissivity and σ is the Stefan-Boltzmann constant, B_1 and B_2 are from reference [30]. The initial temperature for T_{r1}^0 to T_{r5}^0 are kept constant at 70 K same as LN_2 inlet temperature.

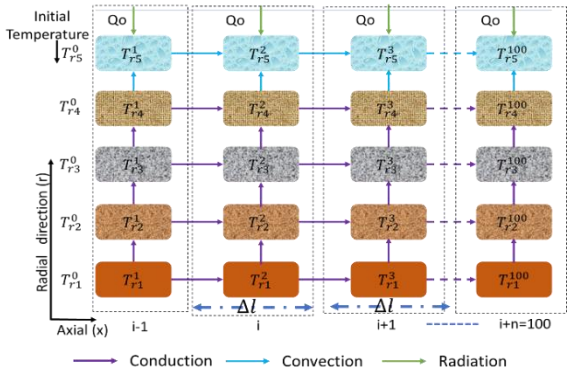

Fig. 2. Discretized electrical-thermal model of the HTS cable

The HTS cable is divided into 100 subsections i.e. 100 pi sections (1 km long each) in the cable model and its electrical equivalent circuit as shown in Fig. 3(a). The heat transfer through the layers by conduction, and convection is used in each element, and the consequent elements are considered in this modelling to get electrical and thermal characteristics of the DC HTS cable under different fault locations. In our model, we posited that the flow of liquid nitrogen (LN_2) initiates at the 0 km mark, extending to 5 km as the endpoint, before returning to the cryocooler via a distinct return path. We utilized a cryocooler to cool each subsequent 5 km cable segment. This procedure was replicated for every consecutive 5 km section of the cable. We established an initial temperature of 70 K as the boundary condition at the start of each segment, spanning intervals such as 0-5 km, 5-10 km, 10-15 km, and so on, up to the 95-100 km cable section as shown in Fig. 3(a). A joint was considered for each one-kilometer cable segment.

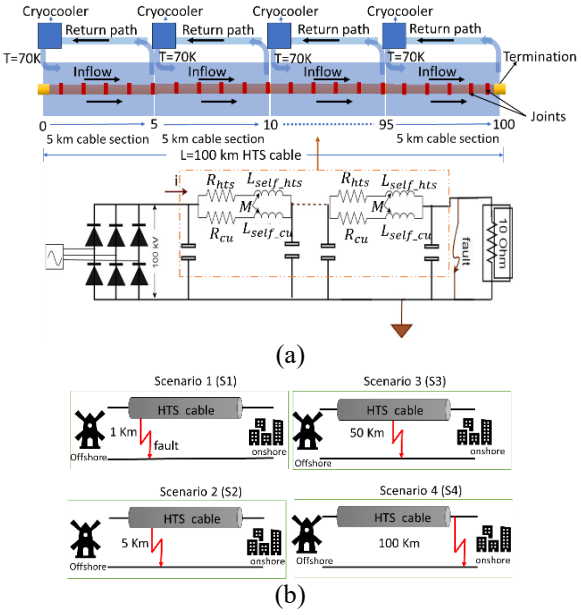

Fig. 3. (a) Electrical equivalent circuit used in the Discretized MATLAB/SIMSCAPE model with the cooling system arrangement and (b) fault location in the cable scenarios.

III. Results and Discussion

The simulation results show the temperature of the superconductor varies along the cable, ranging from 70 K to 73.8 K for each 5 km section. The critical current (Ic) of the superconductor is influenced by the cable's temperature. A total of 20 cryocoolers were used for the 100 km long cable. Initially, the Ic of the cable is 22.2 kA, but it decreases to 18 kA at the end of the 5 km cable section in the 100 km long cable. The thermal and electrical behaviour of the superconductor follows a repeating pattern for each 5 km cable section, as depicted in Fig. 4(a) and (b) for temperature and Ic respectively. The copper former has a resistance of 1.5 mΩ/km, while the HTS resistance is negligible compared to the copper former. During steady-state conditions, the current flowing through the HTS layers is 10 kA, while the current through the copper former layer is 0 A, due to the high resistance of the copper former.

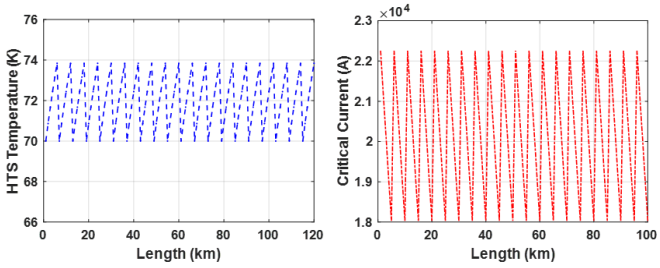

Fig. 4. Under normal operating conditions (a) HTS temperature, (b) critical current of the cable.

The fault occurs due to abnormalities in the dielectric [31] and the length of 2G HTS tapes produced has limitations and needs joints and terminations to connect the cable to the distributed network. An example was the Europe-centered grid mentioned in reference [32]. We conducted fault tests on the superconductor power grid at various locations to investigate the impact of fault location on the thermal and electrical behaviour superconductor. When a fault occurs, the current flowing through the superconductor exceeds the critical current threshold, resulting in an increase in resistance within the HTS tapes. This results in joule heating, causing a rise in temperature within the superconductor, ultimately leading to quenching. During this process, the resistance of the superconductor becomes higher than that of the copper former and consequently shifts current from the superconductor to the copper former.

Changes in the cable's fault location lead to variations in its electrical characteristics. When a fault happens farther from the power source, the cable's fault current is lower than when the fault occurs closer to the generation side. This phenomenon is clearly illustrated in Fig. 5, where a fault occurring in (S1) at 1 km from the source results in the highest fault current amplitude. However, as the fault location shifts to greater distances from the source i.e. Scenarios S2, S3, and S4, the fault current amplitude decreases. Specifically, when the fault is nearer to the power generation side, the current in the cable rises more rapidly, consequently affecting the temperature increase in the superconductor.

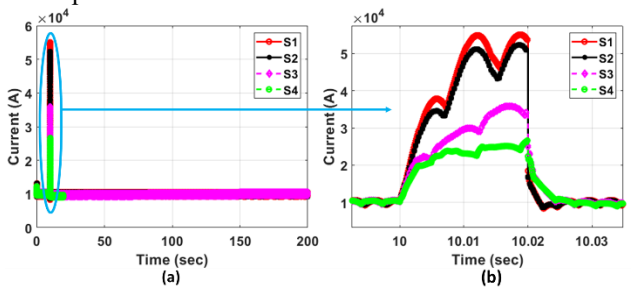

Fig. 5. The current in the cable during fault at different scenarios S1 to S4.

The analysis of current flow within the circuit during a fault at different sections of the cable revealed intriguing insights. The cable pattern for every five-kilometer section was found to be repetitive until the point of the fault in our model. Specifically, a fault occurring at the 5 km point is illustrated in Fig 6, highlighting the corresponding changes in current within the HTS and former layer along the length.

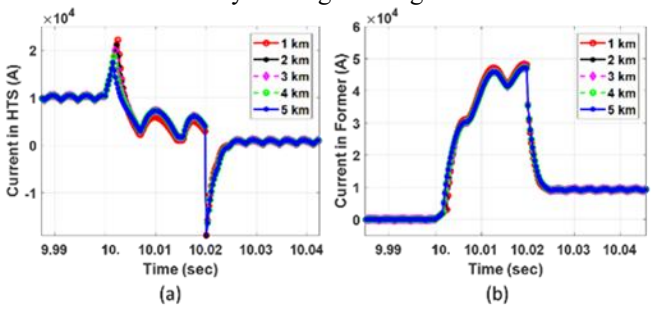

Fig. 6. Current in HTS and copper former during scenario 2.

Specifically, when a fault occurs at the 5 km point (S2), the current in the HTS begins to rise, eventually exceeding 18 kA. At this point, the cable's 4-5 km section experiences quenching, driven by an increase in R_{hts} and i_{hts} decays. Similarly, as the current surpasses 19 kA, the 3-4 km section undergoes quenching, followed subsequently by the 2-3 km, 1-2 km, and 0-1 km sections as their current levels exceed their respective Ic values. In our modelling, we introduced a temporary fault scenario for 20 msec, the short-circuit impedance was 0.01 Ω and after the fault cleared, the current reverted from the short circuit path back to the HTS cable. At this point, we noticed a negative current peak in the HTS layer due to abrupt changes in $M\frac{di_{cu}}{dt}$ as mentioned in equation 3. Even after the fault is cleared, the HTS cable's temperature remains above Tc, and the drifted current flowing in the copper former layer persists until it returns to below Tc.

When the fault occurs at 100 km (S4), the current distribution in the layers is depicted in Fig 7(a) and (b). Its behaviour is similar to the fault at 5 km shown in Fig. 6(a). During the fault, it exhibits a more resistive pathway, effectively limiting the fault current at a maximum of 25.6 kA.

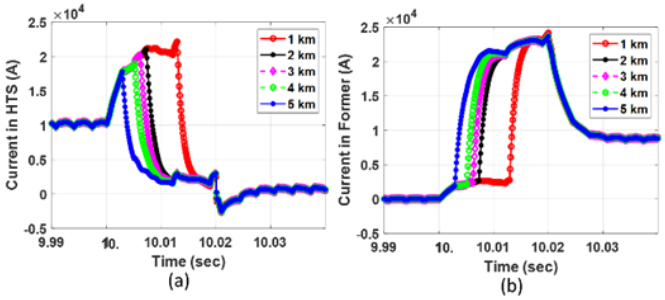

Fig. 7. Current in (a) HTS and (b) copper former during scenario 4 (S4)

Based on the aforementioned analysis, the electrical characteristics are influenced by the fault location, and this also has an impact on thermal behaviour. As depicted in Fig. 8, we observe a variation in the HTS temperature based on fault locations at 5 and 50 km points. Notably, faults occurring closer to the generation side exhibit a more significant thermal impact, with an HTS temperature variation of 20.38 K for faults at 5 (S2) and 50 km (S3) points and for S3 and S4 (100 km) points the temperature variation is 30.15 K. The recovery of the HTS temperature to reach below the critical temperature (<Tc), for the S2 scenario takes approximately 13 seconds longer than the S3 scenario. The temperature of the HTS section that experienced quenching reaches a peak of approximately (T_{r2}^{100}=222.15 K), (T_{r2}^{50}=252.4 K) and (T_{r2}^{5} =272.78 K), taking roughly 144 seconds, 150 seconds and 163 seconds to recover and return to a pre-fault condition, respectively, for faults at 50 and 5 km points. As a result of the fault current within the HTS, the temperature is depicted within the magnified portion on the right side of Figure 8. Subsequently, as the superconductor experiences quenching, the HTS current (i_{hts}) diminishes while the former current (i_{cu}) escalates. Besides the internal heat generated within the HTS layer due to ($i_{hts}^2 R_{hts}$), the temperature further elevates due to heat transfer from the copper former through conduction. This is due to the amplitude

of the current in the cable during the fault condition shown in Fig 5. The joule losses in the cable increase which results in the increases of joule heating. For the fault that occurs near the source takes a longer time to recover to the superconducting state than far faults. The heat generated by the cable's conducting layers causes the LN_2 to undergo boiling. In the stable condition, the LN_2 temperature fluctuates along a 5 km cable section (from $T_{r5}^{1} = 70$ K to $T_{r5}^{5} = 74$ K), during the fault and recovery process, peaks at a maximum (from $T_{r5}^{5} = 75$ K to $T_{r5}^{5} = 80.5$ K). The resistance and joule losses in the HTS layer and copper former are depicted in Fig.9.

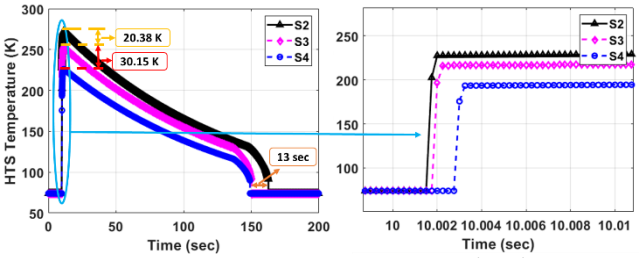

Fig. 8. Temperature of the HTS cable ($T_{r2}^{5}, T_{r2}^{50}, and\ T_{r2}^{100}$) during fault at scenarios S2, S3, and S4 respectively.

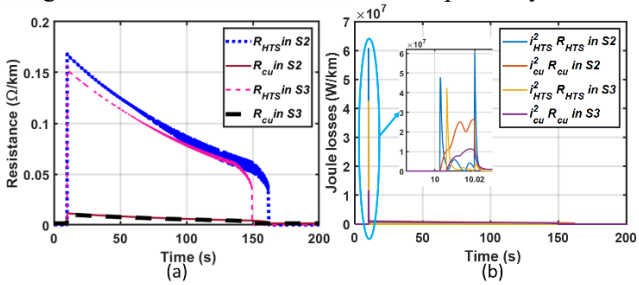

Fig. 9. (a) Resistance and (b) Joule losses during scenarios S2 and S3.

The temperature increase in the copper former is depicted in Fig.10, attributed to the current ramp within the former section as presented in Fig. 6(b). The temperature rise initially commences at the 5 km mark, followed by the 4 km to 1 km segments. From the thermal analysis, it becomes evident that the superconductor requires a significant duration, approximately 2.5 to 3 minutes depending on the fault location, to recover from a quench.

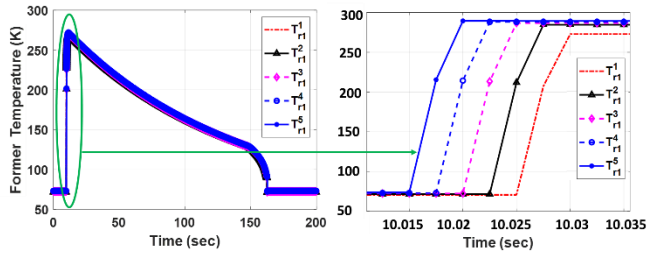

Fig. 10. The temperature of the copper former layer during fault occurs at 5 km (S2).

To mitigate these circumstances, the implementation of a SFCL can be considered. This SFCL serves to restrict the fault current, affording additional time for the DC circuit breaker to trip in the event of a prolonged fault condition. It's self-triggering, returning to normal operation once the fault is cleared and the superconductor cools below the critical temperature, without requiring additional hardware.

The schematic in Fig. 11 illustrates a straightforward design of the resistive superconducting fault current limiter. In this configuration, the High-Temperature Superconductor is linked in parallel with the copper conductor, and an inductor is connected in series with this parallel resistance branch. This setup enhances the transient stability of the power system by mitigating fault currents when faults occur. We incorporated a SFCL into the model depicted in Fig. 3 and then conducted the simulation, introducing a temporary fault lasting 10 msec.

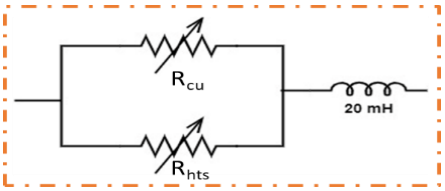

Fig. 11. A simple Resistive fault current limiter

Fig. 12(a) illustrates that, when utilizing the SFCL, the current within the cable is effectively restricted during the fault, maintaining it at 17.5 kA maximum, which is below the cable's critical current (Ic) threshold, thus preserving the superconducting state of the HTS. During the fault, once the current reaches critical current (SFCL Ic=13.9 kA, n_tapes=44), its resistance R_{hts} increases more than R_{cu} and the temperature of the SFCL rises current starts flowing to the R_{cu} path. Fig. 12(b) displays the temperature profile of the HVDC superconductor cable. Conversely, in the circuit without the SFCL, the current surges to 40 kA, leading to the quenching of the HTS cable.

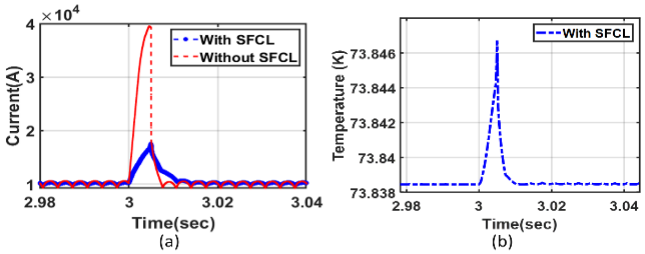

Fig. 12. (a) current in the cable with and without SFCL and (b) HTS temperature of 4-5 km section with SFCL

IV. Conclusion

The investigation focused on analyzing the effects of faults at different points within the superconducting power cable grid. The results revealed significant variations in both thermal and electrical behaviour depending on the location of the fault. The study also examined the current sharing between the HTS and copper former, highlighting how the fault's location affects the amplitude of these currents. Furthermore, the evaluation of superconductor temperature and quench recovery based on fault location provided valuable insights. The use of the SFCL in conjunction with the HTS cable limited the fault current and prevented the HTS from quenching. These findings contribute to a deeper understanding of the behaviour of superconducting power cables during faults and offer valuable insights for the design and operation of such systems in real-world grid applications.

REFERENCES

[1] J. F. Maguire *et al.*, "Progress and status of a 2G HTS power cable to be installed in the Long Island Power Authority (LIPA) grid," *IEEE Transactions on Applied Superconductivity*, vol. 21, no. 3 PART 2, pp. 961–966, 2011, doi: 10.1109/TASC.2010.2093108.

[2] R. Soika, X. G. Garcia, and S. C. Nogales, "ENDESA Supercable, a 3.2 kA, 138 MVA, medium voltage superconducting power cable," *IEEE Transactions on Applied Superconductivity*, vol. 21, no. 3 PART 2, pp. 972–975, 2011, doi: 10.1109/TASC.2010.2100357.

[3] M. Stemmle, F. Merschel, M. Noe, and A. Hobl, "Plenary talk - European project and application of high Tc superconducting cable," *2013 IEEE International Conference on Applied Superconductivity and Electromagnetic Devices, ASEMD 2013*, p. 257, 2013, doi: 10.1109/ASEMD.2013.6780759.

[4] T. Masuda *et al.*, "Fabrication and installation results for Albany HTS cable," *IEEE Transaction on Applied Superconductivity*, vol. 17, no. 2, pp. 1648–1651, 2007.

[5] D. C. Superconducting and P. Cables, "Concept and Design of 500 Meter and 1000 Meter DC Superconducting Power Cables in Ishikari, Japan," *IEEE Transactions on Applied Superconductivity*, vol. 25, no. 3, pp. 3–6, 2015.

[6] D. Zhang *et al.*, "Stability Analysis of the Cable Core of a 10 kA HTS DC Power Cable Used in the Electrolytic Aluminum Industry," *IEEE Transactions on Applied Superconductivity*, vol. 25, no. 3, pp. 1–4, 2015, doi: 10.1109/TASC.2014.2374691.

[7] V. Sytnikov, A. Kashcheev, M. Dubinin, V. Karpov, and T. Ryabin, "Test Results of the Full-Scale HTS Transmission Cable Line (2.4 Km) for the St. Petersburg Project," *IEEE Transactions on Applied Superconductivity*, vol. 31, no. 5, 2021, doi: 10.1109/TASC.2021.3063067.

[8] B. Yang, J. Kang, S. Lee, C. Choi, and Y. Moon, "Qualification Test of a 80 kV 500 MW HTS DC Cable for Applying into Real Grid," *IEEE Transactions on Applied Superconductivity*, vol. 25, no. 3, 2015, doi: 10.1109/TASC.2015.2396683.

[9] J. H. Lim *et al.*, "Cryogenic system for 80-kV DC HTS cable in the KEPCO power grid," *IEEE Transactions on Applied Superconductivity*, vol. 25, no. 3, Jun. 2015, doi: 10.1109/TASC.2014.2387393.

[10] B. Wang *et al.*, "Design, Manufacture, and Test of a 30 m 10 kV/2.5 kA Concentric HTS Cable Prototype for Urban Grid," *IEEE Access*, vol. 9, pp. 120066–120077, 2021, doi: 10.1109/ACCESS.2021.3108199.

[11] S. Tang *et al.*, "Development and demonstration of concentric-type HTS power cable for distribution grid in Shenzhen urban," *Frontiers in Energy Efficiency*, vol. 1, p. 1160372, 2023.

[12] X. H. Zong, Y. W. Han, and C. Q. Huang, "Introduction of 35-kV kilometer-scale high-temperature superconducting cable demonstration project in Shanghai," *Superconductivity*, vol. 2, p. 100008, 2022, doi: https://doi.org/10.1016/j.supcon.2022.100008.

[13] Y. Ohki, "News From Japan Development of a 6-kV, 3,000-A Triaxial Superconducting Cable." IEEE-INST ELECTRICAL ELECTRONICS ENGINEERS INC 445 HOES LANE, PISCATAWAY, NJ …, 2022.

[14] "'ComEd and AMSC Announce Successful Integration of Resilient Electric Grid System in Chicago'', AMSC, Aug. 31, 2021. https://www.amsc.com/comed-and-amsc-announce-successful-integration-of-resilient-electric-grid-system-in-chicago/ (accessed Apr. 15, 2022).'".

[15] D. Guillen, C. Salas, F. Trillaud, L. M. Castro, A. T. Queiroz, and G. G. Sotelo, "Impact of Resistive Superconducting Fault Current Limiter and Distributed Generation on Fault Location in Distribution Networks," *Electric Power Systems Research*, vol. 186, p. 106419, 2020, doi: https://doi.org/10.1016/j.epsr.2020.106419.

[16] G. Gonçalves Sotelo *et al.*, "A review of superconducting fault current limiters compared with other proven technologies," *Superconductivity*, vol. 3. Elsevier B.V., Sep. 01, 2022. doi: 10.1016/j.supcon.2022.100018.

[17] M. Moyzykh *et al.*, "First Russian 220 kV Superconducting Fault Current Limiter (SFCL) for Application in City Grid," *IEEE Transactions on Applied Superconductivity*, vol. 31, no. 5, Aug. 2021, doi: 10.1109/TASC.2021.3066324.

[18] X. Chen *et al.*, "Superconducting fault current limiter (SFCL) for fail-safe DC-DC conversion: From power electronic device to micro grid protection," *Superconductivity*, vol. 1, Mar. 2022, doi: 10.1016/j.supcon.2022.100003.

[19] M. Song *et al.*, "Design and performance tests of a 160 kV/1.0 kA DC superconducting fault current limiter," *Physica C: Superconductivity and its Applications*, vol. 585, p. 1353871, 2021, doi: https://doi.org/10.1016/j.physc.2021.1353871.

[20] C. Liang *et al.*, "Winding Technology and Experimental Study on 500 kV Superconductive Fault Current Limiter," *IEEE Transactions on Applied Superconductivity*, vol. 28, no. 3, Apr. 2018, doi: 10.1109/TASC.2018.2805722.

[21] G. Del-Rosario-Calaf, J. Lloberas-Valls, A. Sumper, X. Granados, and R. Villafafila-Robles, "Modeling of second generation HTS cables for grid fault analysis applied to power system simulation," *IEEE Transactions on Applied Superconductivity*, vol. 23, no. 3, 2013, doi: 10.1109/TASC.2012.2236673.

[22] E. Tsotsopoulou *et al.*, "Modelling and fault current characterization of superconducting cable with high temperature superconducting windings and copper stabilizer layer," *Energies (Basel)*, vol. 13, no. 24, Dec. 2020, doi: 10.3390/en13246646.

[23] T. T. Nguyen *et al.*, "A simplified model of coaxial, multilayer high-temperature superconducting power cables with Cu formers for transient studies," *Energies (Basel)*, vol. 12, no. 8, Apr. 2019, doi: 10.3390/en12081514.

[24] R. Su *et al.*, "Numerical Model of HTS Cable and Its Electric-Thermal Properties," *IEEE Transactions on Applied Superconductivity*, vol. 29, no. 5, Aug. 2019, doi: 10.1109/TASC.2019.2901874.

[25] X. Li *et al.*, "Simulation Analysis of 2D Finite Element Axial Transient Temperature Distribution of HTS Cable," *IEEE Transactions on Applied Superconductivity*, vol. 31, no. 5, Aug. 2021, doi: 10.1109/TASC.2021.3061344.

[26] N. M. Strickland, C. Hoffmann, and S. C. Wimbush, "A 1 kA-class cryogen-free critical current characterization system for superconducting coated conductors," *Review of Scientific Instruments*, vol. 85, no. 11, Nov. 2014, doi: 10.1063/1.4902139.

[27] N. Duan, W. Xu, S. Wang, and J. Zhu, "Current Distribution Calculation of Superconducting Layer in HTS Cable Considering Magnetic Hysteresis by Using XFEM," *IEEE Trans Magn*, vol. 54, no. 3, 2018, doi: 10.1109/TMAG.2017.2751257.

[28] S. K. Olsen, C. Traeholt, A. Kuhle, O. Tonnesen, M. Daumling, and J. Ostergaard, "Loss and inductance investigations in a 4-layer superconducting prototype cable conductor," *IEEE Transactions on Applied Superconductivity*, vol. 9, no. 2, pp. 833–836, 1999, doi: 10.1109/77.783426.

[29] P. Chaganti, W. Yuan, M. Zhang, L. Xu, E. Hodge, and J. Fitzgerald, "Modelling of a High-Temperature Superconductor HVDC Cable Under Transient Conditions," *IEEE Transactions on Applied Superconductivity*, vol. 33, no. 5, pp. 1–5, 2023, doi: 10.1109/TASC.2023.3251948.

[30] J. A. Souza, J. C. Ordonez, R. Hovsapian, and J. V. C. Vargas, "Thermal modeling of helium cooled high-temperature superconducting DC transmission cable," *IEEE Transactions on Applied Superconductivity*, vol. 21, no. 3 PART 2, pp. 947–952, Jun. 2011, doi: 10.1109/TASC.2010.2099196.

[31] J. Gerhold and T. Tanaka, "Cryogenic electrical insulation of superconducting power transmission lines: transfer of experience learned from metal superconductors to high critical temperature superconductors," *Cryogenics (Guildf)*, vol. 38, no. 11, pp. 1173–1188, 1998, doi: https://doi.org/10.1016/S0011-2275(98)00105-2.

[32] M. Cullinane, F. Judge, M. O'Shea, K. Thandayutham, and J. Murphy, "Subsea superconductors: The future of offshore renewable energy transmission?," *Renewable and Sustainable Energy Reviews*, vol. 156. Elsevier Ltd, Mar. 01, 2022. doi: 10.1016/j.rser.2021.111943.